ACS APPLIED MATERIALS & INTERFACES

Research Article

www.acsami.org

Substrate and Thickness Effects on the Oxygen Surface Exchange of $La_{0.7}Sr_{0.3}MnO_3$ Thin Films

Lu Yan and Paul A. Salvador*

Department of Materials Science and Engineering, Carnegie Mellon University, 5000 Forbes Avenue, Pittsburgh, Pennsylvania 15213, United States

Supporting Information

ABSTRACT: Substrate- and thickness-related effects on the oxygen surface exchange of $La_{0.7}Sr_{0.3}MnO_3$ (LSM) thin films were investigated to understand better cathode reactivity in solid oxide fuel cells. Epitaxial (100)-oriented LSM films were fabricated on (100)-$SrTiO_3$ and (110)-$NdGaO_3$ substrates and were characterized using electrical conductivity relaxation. A strong substrate effect on the chemical surface exchange coefficient (k_{chem}) was observed, with a higher k_{chem} found for films on $SrTiO_3$ than those on $NdGaO_3$. Two distinct activation energies (E_a) were observed for k_{chem}, which were assigned to two parallel exchange processes; the relative contributions from each depended on the substrate, film thickness, and temperature. For films coherently strained to the substrates, k_{chem} values differed by almost an order of magnitude, whereas E_a was ~1.5 (± 0.1) eV on both substrates. For relaxed films, k_{chem} values differed only by a factor of 2, and E_a was ~0.75 (± 0.1) eV on both substrates. We discuss the strain effect relative to the native surface exchange and the thickness effect relative to the extended defect populations in the films. The outcome of this study sheds light on how microstructural features affect surface chemistry in modified cathodes.

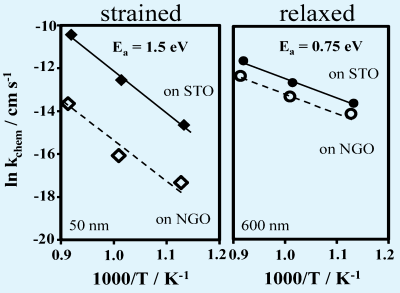

KEYWORDS: *surface exchange, thin films, strain, dislocations, solid oxide fuel cells, (La,Sr)MnO_3*

1. INTRODUCTION

An improved understanding of the complex oxygen reduction reaction (ORR) that occurs in the cathodes of solid oxide fuel cells (SOFCs) is needed to enhance the overall cell efficiency and lower the total cost.[1−3] Research on the development of cathodes that facilitate both oxygen surface exchange and bulk oxide ion transport has therefore attracted extensive attention.[2−7] Thin film samples have been used to study surface exchange, especially the surface exchange coefficient k, because of the control they afford over electrode geometric features,[8,9] surface crystallographic orientations,[10−12] strain states,[5,13,14] and microstructural features.[11,15,16] However, it is well-known that films often exhibit very different volumetric properties than bulk materials owing to the different stoichiometries, strains, extended defects, and thicknesses/geometries, as well as other possible influences from the substrate. Many reports that used thin films for surface measurements focused on measurements taken from a single film or a single type of film with different electrode geometries.[9,15−17] Owing to this, it remains unclear how to correlate surface properties measured on specific films to those measured for bulk materials. In this work, we compare surface properties measured for films on different substrates and of different thicknesses, which primarily influence the strain state and dislocation content, to correlate film properties to these underlying materials parameters.

Perhaps the most extensive sets of work in understanding surfaces of cathode thin films has focused on understanding surface segregation and overall composition variations in thin films, because cation segregation, oxygen vacancies, and adsorbates are often cited as the most relevant considerations for surface oxygen exchange. Sr segregation to the surface in Sr-doped perovskite cathodes has received particular attention. For most studies using bulk materials, a decrease in the activity was correlated to increased Sr concentrations and Sr surface segregation was observed to be a function of temperature and electrochemical loads.[18−22] For thin film samples, Sr-segregation has also been widely observed[23−28] and is a function of temperature[24,25] and electrochemistry.[26] The correlation to activity is less clear, though correlations of surface composition with electrochemistry are documented for $(La,Sr)(Co,Fe)O_3$.[29] Whether such segregation is correlated to the strain state is unclear since some reports indicate that it is[28] some reports indicate it is not.[23,24] Computational investigations were used to support Sr segregation to the (100) surface for both strain states, yet the segregation increased as the strain changed from compressive to tensile values in computations.[28] The differences observed experimentally are likely a result of sample-to-sample variation or experimental measurement precision. Oxygen vacancy concentration variations in oxygen vacancy rich perovskite films, such as $LaCoO_3$ based materials, have also been widely studied. Strain has been shown to impact defect formation energies,[30,31] oxygen vacancy order,[32] as well as long-range cation ordering[33] in perovskite cobaltites. In this report, we aim to directly measure the effect

Received: February 10, 2012
Accepted: May 2, 2012
Published: May 2, 2012

of strain on surface exchange, as an initial step toward linking the above-described strain-dependent chemical effects to overall surface properties.

Recent studies have revealed interesting thickness and substrate effects on the oxygen surface activity of films (described below). While no conclusive understanding has yet been obtained, largely because systematic studies that control explicitly the underlying actors are lacking, these initial observations indicate that the surface exchange measured on thin films of nominally the same material vary widely. For example, the chemical surface exchange coefficient, k_{chem}, of $La_{0.8}Sr_{0.2}CoO_3$ films on yttria-stabilized zirconia (YSZ), was found to increase with a decrease in film thickness and k_{chem} values of thin films were up to 2 orders of magnitude higher than those measured on bulk materials.[5] In contrast, an increase in k_{chem} was observed with thickness for $La_2NiO_{4+\delta}$[13] and gallia-doped ceria[34] films. For epitaxial $YBa_2Cu_3O_{7-x}$[35] and textured $La_{0.7}Sr_{0.2}MnO_3$[36] films, two distinct and measurable k_{chem} values were observed. Recently, we showed that both the value of k_{chem} and its activation energy were a function of surface orientation for epitaxial, relaxed $La_{0.7}Sr_{0.3}MnO_3$ (LSM herein) films.[12,37] Even simply annealing a $La_{0.5}Sr_{0.5}CoO_3$ film at high temperatures led to a 2 orders of magnitude increase in the measured k_{chem}.[38] In each case, some combination of strain, overall and surface compositions, extended defect populations, and/or surface roughness was implicated as an important actor in oxygen exchange. What this collection of film work indicates is that compositional, microstructural, substrate related, and orientational effects all play a role in determining k_{chem}, and must be considered independently to understand activity.

In this study, we isolate the surface response from the bulk diffusion properties using epitaxial thin films and measure the exchange kinetics with electrical conductivity relaxation (ECR). A discussion comparing k_{chem} and D_{chem}, as extracted from ECR data on 600 nm thick LSM films, and justifying the isolation of the surface property is found elsewhere.[12,37] Epitaxial (100) $La_{0.7}Sr_{0.3}MnO_3$ (LSM) thin films are deposited on $SrTiO_3$ (STO) and $NdGaO_3$ (NGO) single crystals by pulsed laser deposition (PLD) and k_{chem} is measured versus film thickness, substrate, and temperature. Changes in both k_{chem} and its activation energy E_a with thickness, substrate, and temperature are related to strain and extended defect (dislocation) concentrations. Our results suggest that substrate related tensile strains and large extended defect populations (dislocation densities) lead to surface exchange rates that are much greater than those for bulk LSM materials. We discuss these results to the use of LSM as catalysts supported on other cathodes, such as in infiltrated SOFC cathodes.[6,39,40]

2. EXPERIMENTAL SECTION

50 to 600 nm thick, perovskite LSM thin films were deposited by pulsed laser deposition (PLD).[12,24,26,37] A KrF excimer laser (λ = 248 nm) was pulsed at 1 to 3 Hz and focused on a ceramic target, of nominal composition $La_{0.7}Sr_{0.3}MnO_3$, to yield an areal energy density of 2 J/cm^2. We used 10 mm × 10 mm × 0.5 mm coupons of (100)-oriented STO and (110)-oriented NGO single crystals (purchased from MTI Corporation, USA) as substrates; they were cleaned in ultrasonic baths of acetone followed by methanol, for 5 min each.[12,41] Films were deposited at 750 °C under 50 mTorr O_2 with a target to substrate distance of ~60 mm. Film growth rates were determined from thickness measurements made using X-ray reflectometry (XRR),[42,43] and film thicknesses were controlled by depositing an appropriate number of pulses.

Phase identification, epitaxy, strain state, and the out-of-plane orientation spread (related to dislocation content) were characterized by X-ray diffraction (XRD) (in θ–2θ, φ, and ω scan modes), all using a Philips X'Pert MRD (λ = 1.5418 Å, Cu K_α).[42,43] High-resolution XRD was carried out using a hybrid optical module for lattice parameter calculation as well as for rocking curve scans.[44] The out-of-plane and in-plane lattice parameters were determined from the XRD data based on the angular positions of different *hkl* reflections.[44] The surface morphology of the films was investigated using ex situ atomic force microscopy (Veeco Dimension 3100) in tapping mode on an area of 2 μm × 2 μm.[44]

Electrical conductivity was measured in a four-point van der Pauw configuration, with Au as the contact to LSM, using a Keithley 2182A nanovoltmeter and a Keithley 6620 precision current source, which was set to deliver 1 mA current.[12,37] Conductivity measurements were carried out in oxygen pressures from 50 mTorr to 500 mTorr at temperatures of approximately 600 to 900 °C. In most transient experiments, the oxygen pressure (PO_2) was changed between 50 mTorr and 500 mTorr, using the mass flow controller (smaller steps in pO_2 were also taken, but the k_{chem} values did not vary significantly while the noise increased for small steps at low temperatures). In electrical conductivity relaxation (ECR) experiments, the relative changes in the electrical conductivity following an abrupt change in pO_2 (from 50 to 500 mTorr for oxidation; 500 to 50 mTorr for reduction) were measured. ECR data could be modeled on the basis of a surface exchange model with a single surface exchange coefficient. k_{chem} was obtained based on fitting the data of the relaxation curves and corrected by taking account of the chamber flush time. Details regarding the ECR experiment set-ups and data analysis are explained elsewhere[12,37] (as used to investigate 100 to 600 nm thick LSM films). The mathematical relationships between electrical conductivity and surface exchange coefficient are given as follows[11,35,38,45]

$$g(t) = \frac{\sigma_t - \sigma_{initial}}{\sigma_{final} - \sigma_{initial}} = 1 - \exp\left(-\frac{k_{chem}t}{L}\right) = 1 - \exp\left(-\frac{t}{\tau}\right) \quad (1,)$$

where $g(t)$ is the normalized conductivity, σ_t is the conductivity at time t, σ_{final} is the conductivity at re-equilibrium, $\sigma_{initial}$ is the conductivity at the initial state, τ is a relaxation time constant and L is the sample thickness. A least-squares approach was used to fit individual curves and to extract k_{chem}. A typical set of data and the fit to that data is given elsewhere[37] and in Supporting Information, Figure S1.

3. RESULTS

3.1. Structural Characterization of Films. As expected,[12,37,46] the pseudocubic (pc) film epitaxy was found to be $(100)[010]_{film} \| (100)[010]_{substrate}$ (determined using XRD methods described elsewhere for similar $La_{0.7}Sr_{0.3}MnO_3$ films on $SrTiO_3$[12]). For relaxed (thick) $La_{0.7}Sr_{0.3}MnO_3$, the pc approximation with $a_{pc} \approx 3.876$ Å is reasonable since $La_{0.7}Sr_{0.3}MnO_3$ has only a slight rhombohedral distortion.[47−52] $SrTiO_3$ is cubic with a = 3.905 Å.[53,54] $NdGaO_3$ has a significant orthorhombic (O) distortion; the Pbnm structure has lattice parameters of: a = 5.43 Å, b = 5.5 Å, and c = 7.71 Å.[55−59] The orthorhombic (110) surface plane is equivalent to a $(100)_{pc}$ plane. The equivalent pc in-plane lattice parameters are $b_{PC} \approx 3.864$ Å $= 1/2[1\bar{1}0]_O$ and $c_{PC} = 3.855$ Å $= 1/2c_O$. For thick films, a more accurate description of the two degenerate epitaxial arrangements on $NdGaO_3$ are $(100)[010]_{film,pc} \| (110)[1\bar{1}0]_{NGO,O}$ and $(100)[010]_{film,pc} \| (110)[001]_{NGO,O}$, which are both equivalent to the pc cube-on-cube geometry.

The lattice parameters and overall strain states determined from high-resolution XRD of LSM films are reported as a function of thickness in Tables 1 and 2, respectively, for films on STO and NGO. The 50 nm thick film on STO exhibits an in-plane lattice parameter that is larger than the bulk values and

Table 1. Lattice Parameters of LSM Films on STO[a]

thickness (nm)	out-of-plane c (Å)	in-plane a (Å)	tensile strain state[b]
50	3.848	3.905	C
100	3.848	3.899	H
300	3.862	3.870	L
600	3.867	3.873	R

[a]Determined from the location of the $(002)_{pc}$ and $(022)_{pc}$ reflections. [b]C = coherent, H = heavy, L = light, R = relaxed strain state.

Table 2. Lattice Parameters of LSM Films on NGO[a]

thickness (nm)	out-of-plane c (Å)	in-plane a (Å)	in-plane b (Å)	compressive strain state[b]
50	3.904	3.855	3.864	C
100	3.902	3.859	3.870	H
200	3.900	3.862	3.873	M
600	3.885	3.868	3.875	L

[a]Determined from the location of the $(002)_{pc}$ and $(022)_{pc}$ reflections. [b]C = coherent, H = heavy, M = moderate, L = light strain state.

matches that of the substrate, indicating that the film is coherently (C) strained. The out-of-plane lattice parameter is smaller than the bulk values owing to Poisson contraction. As the film thickness is increased for films on STO, the in-plane (out-of-plane) lattice parameter decreases (increases) toward the bulk value owing to the relaxation of the in-plane tensile misfit strain. Such relaxations are well-known to be dislocation−mediated processes.[48] The expected critical thickness for strain relaxation has been reported to be ∼100 nm for $La_{0.7}Sr_{0.3}MnO_3$ on STO;[50] this matches closely the ∼130 nm calculated based on a energy balance model.[60] As observed in Table 1, the relaxation of the lattice parameter is gradual from 100 to 600 nm, where the 600 nm film is essentially fully relaxed (R), though the out-of-plane lattice parameter is smaller than the in-plane parameter by 0.005 Å (± 0.001 Å). The 100 and 300 nm thick films are listed as heavily (H) and lightly (L) strained as their lattice parameters are 0.15% (H) to 0.9% (L) different than for the coherently strained film, but not those of the bulk.

For 50 nm LSM films on NGO, the in-plane lattice parameter is smaller than the bulk values and matches that of the substrate, indicating that the film is also coherently (C) strained (approximately −0.2% to −0.4% in plane). The out-of-plane lattice parameter is larger than the bulk values because of Poisson expansion. Because the two in-plane directions of the NGO substrate are slightly different,[14,46,61] we listed the film lattice parameters for both directions in Table 2 from high-resolution XRD determination. As the film thickness increases, the in-plane (out-of-plane) lattice parameter increases (decreases) toward the bulk value owing to the relaxation of the in-plane compressive misfit strain. The expected critical thickness for strain relaxation is 100 to 150 nm[62] for $La_{0.7}Sr_{0.3}MnO_3$ on NGO. As observed in Table 2, the relaxation of the lattice parameter is gradual from 200 to 600 nm, and the 600 nm film is still lightly strained (L). The 100 and 200 nm thick films are listed as heavily (H) and moderately (M) strained as their lattice parameters are 0.1% (H) to 0.2% (M) different than for the coherently strained film, and not yet equal to the bulk. Figure 1 presents the XRD rocking curves (ω scans) for 50 nm (dotted curves) and 600 nm (solid curves) LSM films on STO (lower curves) and NGO (upper curves) substrates. The rocking curve widths are an indication of the

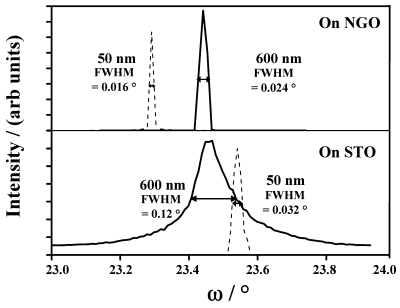

Figure 1. X-ray diffraction rocking curves of 50 and 600 nm $La_{0.7}Sr_{0.3}MnO_3$ (LSM) films on different substrates: (upper) (002) peak of LSM films on $NdGaO_3$;[55] (lower) (002) peak of LSM films on $SrTiO_3$ (STO). fwhm of each peak was marked in the plot.

crystalline quality, being a direct measure of the amount of misorientation of lattice plane normals around their average direction.[63] The full width at half-maximum (fwhm) values for the 50 nm thick films were extremely narrow, being 0.016° on NGO and 0.032° on STO. The fwhm measured[41] for the substrates were ∼0.03° for STO and 0.008° for NGO. These observations indicate that the coherently strained films have crystalline qualities that are nearly identical to those of the substrate. The separation in the peak locations on the ω axis for the 50 nm films arises from the different out-of-plane lattice parameters (the 2θ values used to register these peaks were 46.47 and 47.08° on NGO and STO, respectively) for these coherently strained films. We previously reported such high crystalline qualities for similar thin films on various substrates.[24] Using synchrotron X-ray diffraction experiments[24] on those similar films, it was shown that the crystalline quality and surface smoothness was maintained to 800 °C, indicating the room temperature measurements are reasonable indicators of the state of the film at high temperatures, with the exception of thermal expansion impacting the quantitative values of parameters.

The fwhm values for the 600 nm thick films were much larger, being 0.024° on NGO and 0.12° on STO. These observations indicate that the crystalline quality of the relaxed films are strongly dependent on the substrate. The similarity in the peak locations on the ω axis for the 600 nm films is reflective of the nearly similar out-of-plane lattice parameters for these relaxed films (the 2θ values used to register these peaks were 46.78° and 46.71° on NGO and STO, respectively). The larger fwhm values for films on STO than those on NGO, implies that local (001) plane normals are more widely distributed in space on STO than on NGO. For epitaxial films, the fwhm is a good indication of the dislocation density,[64,65] implying that the films on NGO have lower dislocation (extended defect) content at all thicknesses than on STO. This observation for the thick films is attributed to the better lattice match between LSM and NGO (approximately −0.3%) than between LSM and STO (approximately +0.8%). The number of misfit dislocations required to relax the strain is larger for STO, and this generally causes an increase in the number of threading dislocations (extended defects) that remain in the relaxed films. These threading dislocations, whether isolated or bundled, increase the fwhm of the films.

3.2. Surface Morphology of LSM Films. AFM images registered from (a, b) 50 nm and (c, d) 600 nm thick LSM films deposited on (a, c) STO and (b, d) NGO substrates are given in Figure 2. These images are representative of those

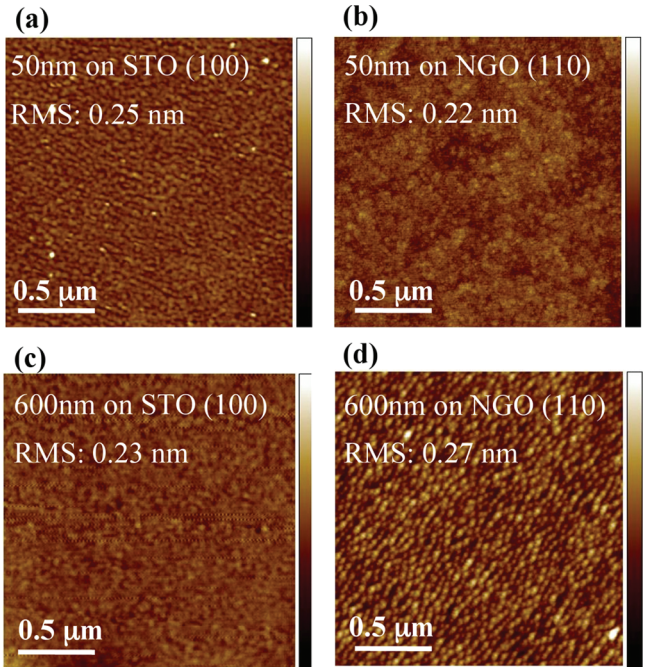

Figure 2. AFM images of four LSM films: (a) 50 nm thick on STO, (b) 50 nm on NGO, (c) 600 nm on STO, and (d) 600 nm LSM on NGO. The root-mean-square roughness over the total area is given in each image. The color scale for all images range from 0 to 3 nm.

observed over the entire film, and for other films measured herein. In each case, the films were observed to be uniform, dense, and smooth, with root-mean-square (rms) surface roughnesses of ~0.25 nm. All observations of similar films yielded results where the rms roughnesses were 0.4 ± 0.2 nm; these values are typical of PLD-prepared films.[12,25] Surface roughness is known to impact surface diffusion,[66] where adatom/adsorbate diffusion is lower on rough surfaces,[67] but this should not be a factor in comparing the results from our films. The total surface areas are also very similar for all films measured here. As measured for the AFM images in Figure 2, the total film surface area varies only by 0.1% of the scanning projection areas (4 μm^2). The film surface morphology is closely related to the total surface area available to participate in the oxygen surface exchange during our ECR experiments. It has been discussed elsewhere that surface roughness affects the measured k_{chem} value for bulk ceramic specimens (and possibly for films[13]), with rougher surfaces increasing the apparent k_{chem}.[13] The similar roughness values support the idea that the ECR measurements on LSM films used in this study should not be affected by the total surface area variations. Also, the local angular orientation variation compared to the surface [001] normal is below 1°, indicating orientation should not affect the results either.[37]

3.3. Surface Exchange Measured at 600 and 800 °C.

The steady state conductivity values, $\sigma(T,pO_2)$, were collected as a function of temperature ($600 \leq T \leq 900$ °C) and oxygen pressure ($50 \leq pO_2 \leq 500$ mTorr) for all films. In general, our films were consistent with reports on bulk LSM; they exhibit polaronic conduction with $\sigma \approx 200$ S/cm at room temperature and a thermal activation energy of $E_a \approx 0.1$ eV.[68] $\sigma(T, pO_2)$ was found to be independent of the thickness and substrate (see Supporting Information, Figure S2), indicating that the high temperature conductivity was not affected by either strain or dislocation content (or film orientation[37]). The dependence of σ on pO_2 was also consistent with bulk observations, where σ is affected by a change in the carrier concentration with pO_2. The carrier population lies in a transition between being controlled by the Sr-doping and by cation vacancies related to gas phase oxidation.[1,68−70] These results indicate that the defect behavior and electron transport in all films are similar to bulk LSM (and each other), and that differences in k_{chem} should not be related to steady state values.

Figure 3 plots k_{chem} (measured during reduction of the pO_2 from 500 to 50 mTorr) as a function of film thickness t (as log

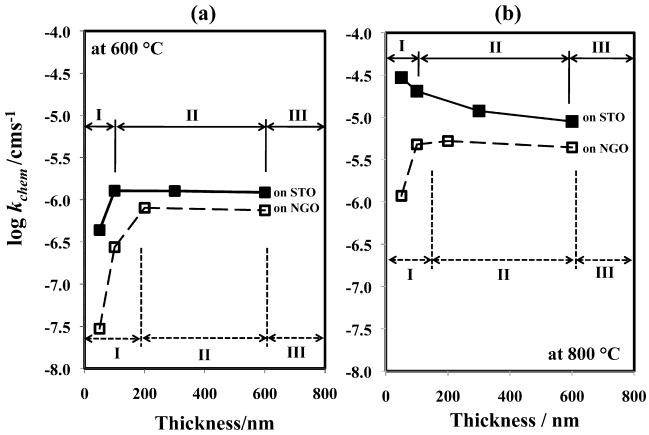

Figure 3. log k_{chem} versus film thickness measured at: (a) 600 and (b) 800 °C. Open (closed) markers are for films on NGO (STO). k_{chem} was measured on changing pO_2 from 500 to 50 mTorr. Estimated regions of different film strain states are separated with dotted (solid) vertical lines for films on NGO (STO), respectively.

k_{chem} vs t) at (a) 600 °C and (b) 800 °C. For most films, no difference was observed between oxidation and reduction (see Supporting Information, Figure S3, and earlier reports[12,37,71]). All data reported and analyzed in this manuscript are for the reduction process. Values for films on STO (NGO) are given in solid (open) symbols. Note that k_{chem} is a function of substrate (s) and thickness. k_{chem} for films on STO are always larger than k_{chem} on NGO. In principle, the surface exchange coefficient should be independent of thickness,[4] but clear and strong deviations from a thickness independent value are observed. What is even more interesting, the magnitude and relative direction of the deviation is a function of substrate and temperature: such behavior is uncommon for films.[5,38,45,72] Nevertheless, k_{chem} tends toward a constant (thickness independent) value as thickness increases, but the thickness where the constant value is obtained depends on temperature while the constant value itself depends on substrate.

Several important points should be made for our systematic investigation. The 50 nm thick films are fully strained. The surface exchange coefficients for those films vary by an order of magnitude at 800 °C. k_{chem} for the films coherently strained in tension to STO is an order of magnitude larger than for the films coherently strained in compression to NGO. The 600 nm thick films are essentially fully relaxed. The surface exchange coefficients are approximately twice as large for films on STO than for films on NGO. Despite these differences, the k_{chem} values observed herein are consistent with the reported values for both thin film and bulk LSM, which range from 3×10^{-6} to 5×10^{-4} cms^{-1},[15,73,74] depending on temperature, pressure, measurement technique, and sample characteristics.

The behavior with thickness is broken down into three regions related to the strain state of the system, denoted with solid (dashed) arrows above (below) the data on STO (NGO) in Figure 3. Films with thicknesses less than (greater than) that denoted by the left (right) arrow represent films that are essentially coherently strained (fully relaxed). Films with thicknesses between those denoted by the arrows represent films that are partially strained, as indicated in Tables 1 and 2. At 600 °C, both partially strained and fully relaxed films have larger k_{chem} values than coherently strained films on both substrates. Films on STO reach their plateau at lower thicknesses than those on NGO. At 800 °C, similar behavior is observed for films on NGO, but the thickness at which the plateau is reached shifts to a lower thickness. In contrast, the coherently strained films on STO have larger k_{chem} values than partially strained and fully relaxed films on STO. In fact, the largest k_{chem} value observed for any film is for the coherently strained films on STO at 800 °C. Another difference for the films on STO at 800 °C is that, although the films measured at 600 °C quickly reach the plateau value with increasing thickness, the films on STO measured at 800 °C reach the plateau at much larger thickness values.

3.4. Temperature Dependence of k_{chem}. The temperature dependence of k_{chem} for LSM on STO (closed symbols) and NGO (open symbols) are given as ln k_{chem} vs $1000/T$ in panels a and b in Figure 4 for 50 and 600 nm thick films,

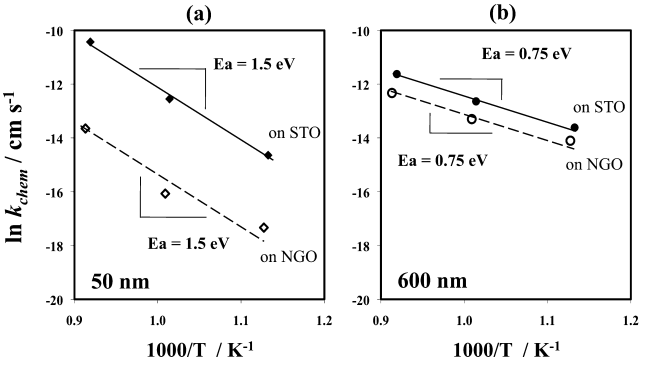

Figure 4. k_{chem} values of LSM films versus inverse temperature: (a) 50 nm films and (b) 600 nm films. Data for films on STO (NGO) are in closed (open) markers and apparent activation energies (E_a marked in images) were fitted with solid (dashed) lines.

respectively. The average behavior of these points was fitted using an Arrhenius relationship, shown with a solid (dashed) line for STO (NGO). The activation energy (E_a) shows a strong thickness dependence but little substrate dependence. 50 nm thick films on both substrates exhibit an activation energy $E_a \approx 1.5 \pm 0.1$ eV. On the other hand, 600 nm thick films on both substrates exhibit an activation energy $E_a \approx 0.75 \pm 0.1$ eV. The different activation energies indicate that the surface exchange of coherently strained films and of fully relaxed films are governed by distinct processes. While the substrate had little effect on E_a over this temperature range, the values of k_{chem} are clearly different. This difference must arise from changes in the pre-exponential term (or the high temperature intercept), discussed later.

The temperature dependence of k_{chem} for LSM on STO (NGO) is given as ln k_{chem} vs $1000/T$ in the main panel (inset) of Figure 5, for all thicknesses. The activation energy measured from the 50 nm coherently strained and 600 nm fully relaxed

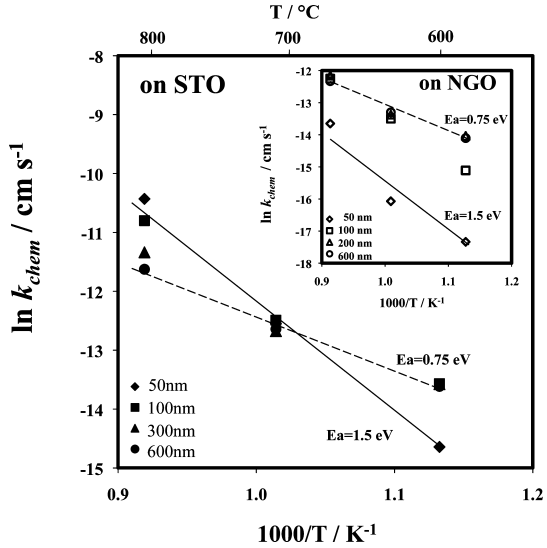

Figure 5. ln k_{chem} versus inverse temperature for films of various thicknesses on STO (inset is for films on NGO). Lines denoting the activation energies of the 50 (600) nm thick films are overdrawn in solid (dotted) lines; their values correspond to E_a = 1.5 (0.75) eV/atom.

films represent the limits of the E_a values observed for all films, and these are also plotted in Figure 5. Depending on the substrate and temperature, the partially strained films exhibit behavior that is either similar to one of the two limiting cases or in a transition between the limits. The LSM film on STO measured at 800 °C gives a good example of this transitional behavior. While partially strained films measured at 600 and 700 °C show thickness independent k_{chem} values similar to the fully relaxed films, a clear thickness dependence to k_{chem} is observed at 800 °C. A similar observation is observed for films on NGO, as shown in the inset of Figure 5. Interestingly, it is at 600 °C that a thickness dependence is observed for the partially strained films indicating a transitional behavior to k_{chem} and E_a. At 700 and 800 °C, the partially strained films are similar to the fully relaxed films.

The existence of two activation energies indicates that two different pathways exist during surface exchange for the LSM films. In addition to the transitional behavior described above, a crossover is observed between the two mechanisms. On STO, the crossover occurs between 700 and 800 °C as indicated in Figure 5. At the higher temperature, the higher activation energy process dominates. On NGO, no crossover point was observed within our measurement conditions, but would exist on extrapolating the lines to higher temperatures. The results in Figure 5 show that both the crossover point and the transitional behavior away from the crossover point are substrate dependent. These observations will be discussed below in relation to a proposed model.

4. DISCUSSION

We observed that the bulk properties of the LSM films were independent of thickness and substrate from 600 to 800 °C (similar to earlier observations[12,37]). In contrast, the electrical and magnetic properties of LSM films measured at low temperature are strongly linked to substrate-induced lattice distortions,[46,75] crystallographic orientation,[75,76] strain related oxygen deficiency,[77] and hole concentrations.[51] This low-temperature behavior arises from strong lattice coupling with

electronic and magnetic order, which greatly affects the critical temperature to both metal−insulator and magnetic transformations. However, the properties measured well above these transformation temperatures (600 °C is well above them) have been found to be similar for films on different substrates and for different thicknesses.[51,76] For highly defective perovskites, such oxygen deficient $LaCoO_3$, strain is known to affect the defect chemistry of films. A strain driven ordering of oxygen vacancies has been reported in $LaCoO_3$ films.[33,78] Our results indicate that the defect chemistry of LSM is less sensitive to strain than $LaCoO_3$, perhaps because LSM is a cation vacancy material with a lower number of overall defects. In any case, this insensitivity to the bulk properties is not reflected in the surface exchange, which is very sensitive to substrate related effects; these are not likely associated with any bulk value change in properties that affect the steady state electronic properties or defect chemistry.

In what follows, we propose a microstructural model to explain the observed k_{chem} dependence on substrate, film thickness, and temperature. Simply put, we propose that the two exchange pathways are associated with (1) the native dislocation-free surface and (2) the surface/bulk region around a dislocation that intersects the surface. By considering the effects of thickness, substrate, temperature, and strain on the relative contribution of these two pathways to exchange, the observations made above can be rationalized and inferences can be made for their impact on cathodes materials. Schematics of three limiting cases expected from the proposed model are given in Figure 6, for a film of thickness L_F.

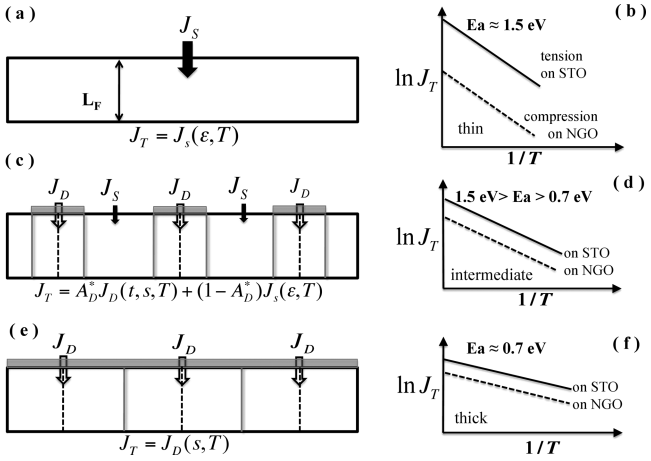

Figure 6. Schematics of the total flux of oxygen during reduction for films wherein: (a) only the native surface contributes, (c) both the native surface and dislocations (vertical dashed lines) contribute, and (e) only the dislocations contribute. The region of the surface (bulk) that each dislocation affects is marked by a gray horizontal (vertical) line. Schematic plots of the corresponding flux (which is proportional to k_{chem}) versus inverse temperature are given in b, d, and f for the surfaces shown respectively in a, c, and e. The activation energies (E_a) model the (b) thin (50 nm), (d) intermediate, and (f) thick (600 nm) films. See text for explanation of terms.

In Figure 6(a), a schematic of surface exchange is given for the native dislocation-free surface. The total flux of oxygen, J_T (atoms/cm^2), will be simply related to the flux across the native surface, J_S (atoms/cm^2). We propose this flux is a function of strain (ε) and temperature: $J_S(\varepsilon,T)$. Keeping in mind that the dislocation content is the lowest for the thinnest films, one expects the dislocation-free surface to be most important in the thinnest films. The 50 nm thick films both exhibited $E_a \approx 1.5$ eV, though the k_{chem} values were strong functions of the substrate. The most likely source of this difference is the coherent strain state differences (see Tables 1 and 2), where LSM on STO (NGO) is in biaxial tension (compression) of ≈ +0.8% (- 0.3%). The rocking curve widths shown in Figure 1 corroborate the low number of dislocations in the coherently strained films. A schematic of measured flux versus inverse temperature for these surfaces are shown in Figure 6(b) (illustrating the same shown in Figure 4(a) for k_{chem}). What is interesting in these observations (and the proposed model) is that strain causes a large difference in the high-temperature intercept of the k_{chem} (or flux) but only a modest, if any, variation in the measured activation energy. We will discuss possible reasons below.

As the films get thicker, the lattice parameters are observed to relax (Tables 1 and 2) gradually until they become fully relaxed above 600 nm. As seen in the rocking curves, the fwhm increases greatly for the 600 nm thick films compared to the 50 nm thick films. Relaxation is largely a dislocation-mediated process, with dislocation propagating from the surface to the interface leaving threading components behind that intersect the native surface. For films in which the dislocation density is large enough, we propose that the entire film can exchange with the gas phase through a dislocation mediated mechanism. In Figure 6(e), a schematic of surface exchange is given for the dislocation-mediated surface. The thick gray surface indicates the portion of the surface that contribute through this path and dislocations are shown as vertical dashed lines. The total flux of oxygen, J_T, is now related to the flux across the surface with intersecting dislocations, J_D (atoms/cm^2).

It should be pointed out that dislocations have long been known to effect heterogeneous catalysis on solid surfaces.[79−84] In oxides, dislocations have been reported to have increased oxygen mobility[85,86] and can exhibit significantly larger oxygen deficiencies than the bulk.[85,87,88] Therefore, dislocations may impact many substeps the overall ORR— adsorption, diffusion, interfacial transfer, and incorporation. Here we show that extended defects associated with relaxation have a measurable effect on the surface exchange, though neither the exact mechanism nor the substep that is modified is known.

We envision that each dislocation impacts a volume of film that is, in a limiting case, related to the spacing between dislocations ($\approx \rho^{-1/2}$, where ρ is the dislocation content in #/cm^2). For 600 nm thick films, the dislocation content should be on the order of 10^{11} cm^{-2}. This would put the spacing between dislocations for most relaxed films as being approximately equal to or less than the films thickness, indicating that such a mechanism should not result in a (lateral) diffusion controlled regime.

We propose that this dislocation flux is a function of substrate (s) and temperature: J_D(s,T), when the films are fully relaxed. The total flux should be related to the total dislocation content (ρ), though the exact relationship of J_d(s,T) on ρ is beyond the scope of this work (and depends on the relative contribution each dislocation makes as the dislocation content increases). We observe that k_{chem} is always lower for relaxed films on NGO than relaxed films on STO (see Figure 4(b)), which is in agreement with the lower dislocation content as reflected in the more narrow rocking curves for films on NGO (Figure 1). The higher crystalline quality of the substrate and the closer lattice match to LSM for NGO compared to STO are

the reasons for the lower dislocation contents on NGO. Importantly, the activation energy related to the dislocation mediated process is relatively insensitive to the substrate, indicating that the number of dislocations affects the pre-exponential term directly, while the activation energy ($E_a \approx$ 0.75 eV) of the dislocation-mediated process is largely unchanged. Note this activation energy is much lower than known for diffusion processes.[89]

While the limiting cases of this model sufficiently explains the data in Figure 4, the transitional behaviors observed for partially strained films observed in Figures 3 and 5 indicate that these two mechanisms must act in parallel (for the model to be appropriate). One expects that each dislocation intersecting the surface can interact with surface species within a surface diffusion length (which should be relative to the exchange rate). The surface diffusion length will be related to surface coverage and diffusion mechanism, both of which are temperature dependent. Similarly, each dislocation can interact with a volume element related to the bulk diffusion (again relative to the time scale of surface exchange), which is also temperature dependent. These two regions are shown in Figure 6(c) around each dislocation; the surface (bulk) that interacts with the dislocation is shown in a gray horizontal (vertical) line (they are set equal to each other here for simplicity sake). The schematic shown in Figure 6(c) indicates a case where only a portion of the surface (bulk) is mediated by dislocations.

In such a transitional case, the total flux J_T will be the area fraction (A^*_D represents the area fraction of the surface controlled by dislocations) summation of the flux through dislocations, $J_D(t,s,T)$, and the flux through native surfaces, $J_S(\varepsilon,T)$, or $J_T = A^*_D\, J_D(t,s,T) + (1\text{-}A^*_D)\, J_S(\varepsilon,T)$. The flux through the dislocations will be dependent on the substrate (s) and thickness, which control the dislocation density, as well as the temperature, which controls the surface/bulk region that interact with a given dislocation. A schematic of an idealized temperature dependence of the flux is given in Figure 6(d), where we simply assumed the area fraction does not change with temperature. In this case, we would measure an intermediate value for the activation energy.

In contrast to the model given in Figure 6(d), the area fraction is not expected to be independent of temperature and we must consider $A^*_D(T)$. The behavior of any given film may be complex, since so many variables exist within even this relatively simple model. The observations of k_{chem} given in Figures 3 and 5 indicate that the behavior is indeed somewhat complex. At low temperatures, the LSM films plateau with thickness for films 100 (200) nm thick on STO (NGO). The plateau with thickness indicates the relative increase in the dislocation content above the plateau thickness value does not further impact the surface exchange. This implies that any given surface area (or bulk volume) is interacting with more than one dislocation, thereby decreasing the impact of marginal increases in dislocation density. Much of the relative increase in dislocation content occurs during the initial relaxation (where the dislocation density increases by many orders of magnitude), while the final relaxation leads to a much smaller relative change. The difference of k_{chem} for films on STO and NGO (which is about a factor of 2) is not expected to be directly related to the dislocation density (which is not likely only a factor of 2, though we did not measure this) in such cases, but there should be some dependence on the dislocation density.

At 600 °C, the 50 nm thick films on STO and NGO are described by the model in Figure 6(a) and the films greater than 100 (200) nm on STO (NGO) are described by the model in Figure 6(e). The 100 nm thick film on NGO is described by the model in Figure 6(c). In this case, the dislocation content is somewhat low and the area fraction of dislocation-mediated surface is less than one. As such, some of the surface is controlled by the slower, higher activation energy process of the compressively strained (100) surface. k_{chem} is therefore observed to be between the limiting values. For this to be the case, the net diffusional processes associated with the dislocation activity must be decreasing with temperature. The implication of this is that at lower temperatures one expects the native surface process to dominate even for the higher dislocation content films, as their area fraction decreases at lower temperatures (assuming no other mechanisms take over).

At 800 °C, the 50 nm thick films on STO and NGO are again described by the model in Figure 6(a) and the films greater than 300 (100) nm on STO (NGO) are described by the model in Figure 6(e). The 100 and 200 nm thick films on STO are described by the model in Figure 6(c). In the latter case, the dislocation content is moderate and, in contrast to the observation that $A^*_D < 1$, the diffusional mechanisms described above are expected to generate $A^*_D = 1$, as observed for the films thicker than 100 nm on NGO at 800 °C. The reason $A^*_D < 1$ for the STO film is related to the crossover in the two parallel processes shown in Figure 5. Since J_S is increasing so quickly with temperature, increased further here by the residual tensile strains, the net value of A^*_D is expected to decrease well above the crossover region observed in Figure 5. This means that the partially strained films in tension (on STO) have a larger high temperature (800 °C) exchange rate owing to greater native surface activity for even moderate dislocation contents. In general, we expect that all films will ultimately be dominated by the native surface properties at sufficiently high temperatures above their corresponding crossover points (assuming no other pathways become active).

Oxygen surface exchange is known to be a complicated process, involving multiple substeps, for which a variety of past reports have discussed potential mechanistic paths. The activation energy for surface diffusion of oxygen on LSM is reported to be 1.34 to 1.65 ± 0.03 eV,[89] which is in a good agreement with our observations for the thin, the fully strained films. Thin films on both substrates exhibit an activation energy $E_a \approx 1.5 \pm 0.1$ eV, which we assign to the native surface. This agreement suggests that our films have a similar rate limiting process, which is possibly surface diffusion limited.[89] We observed that the nature of the substrate had little effect on the activation energy of this surface exchange path but appears to have a strong effect on the pre-exponential factor. A variety of potential mechanisms could be proposed to fit these observations. For example, a small change in the adsorption (defect formation) energies could be caused by strain and could affect the surface concentration of adsorbates (lattice defects), and thereby the number of diffusing species (incorporation sites). This would lead to a large change in the pre-exponential term and a relatively small change in the overall activation energy. Most similar mechanisms would predict some variation in the activation energy concomitant with a change in the pre-exponential term, but the absolute change must remain within our uncertainty.

Strain is known to directly influence the surface structure[23] and surface chemical composition,[24] which would affect surface exchange indirectly. Though Sr-segregation on LSM surfaces have been widely reported, surface compositions were found to

be similar on both strained and relaxed LSM films substrates having both tensile and compressive strain states,[23,24] implying that surface composition is constant with thicknesses and substrate in this study. The activation energy for Sr segregation is below 0.1 eV,[24] which is well within our uncertainty values on k_{chem}, as described above. A more recent study on strain effects on the surface chemical composition revealed that tensile strain indeed favors Sr segregation on the LSM surface more than compressive strains,[27,28] suggesting a possible explanation for the enhanced surface exchange observed in this study, though a Sr-enriched surface is reported be to less active for electron transfer in oxygen reduction reaction.[25] DFT calculations predicted a trend of reduction in oxygen vacancy formation energy and adsorption energy as tensile strain level increases.[31] Epitaxial strains are also shown to influence the LSM surface electronic structure[28] to facilitate the oxygen reactivity at elevated temperatures, owing to surface defect formation and possible reconstructions.[90] Further investigations for each substep in the oxygen reduction reaction is necessary to answer the direct driving force for the enhanced activity of LSM observed on STO.

As for the dislocation-mediated surface, we propose that the incorporation site density becomes fixed and is related to the density of dislocations intersecting the surface. This pre-exponential term likely has a sublinear relation to the actual dislocation content but still plays a role. Therefore, the surface exchange on NGO is always lower than on STO because the dislocation content of LSM on NGO is much lower than of LSM on STO. The lower activation energy likely reflects the change in the incorporation mechanism. At intermediate temperatures, this improves the surface exchange rate. At high temperatures, the native surface overatakes this process owing to the higher activation energy and larger high-temperature intercept. At low temperatures, the region around a dislocation that is controlled by the dislocation decreases sharply, resulting in a return the native surface process as the dominant mechanism.

While the systematic investigation we carried out here shed light on the overall surface exchange mechanisms for LSM, and their relation to strains and extended defect concentrations, the oxygen exchange response is still poorly understood from either a quantitative or a mechanistic perspective of the underlying substeps. There have been relatively few systematic investigations that control the different parameters found here to have dramatic effects on surface exchange, indicating that it is difficult to compare from sample to sample even when clear mechanistic investigation into surface exchange have been carried out. Here alone we observed a 3 orders of magnitude variation in k_{chem} for our nominally similar films, which depends on strain, dislocation content (substrate and thickness), and temperature (see Figure 3). This is not simply a problem of using thin films: similar issues can be discussed relative to bulk samples where grain size and surface roughness are not well controlled, since grain boundaries are expected to behave similar to the dislocations studied herein. In an earlier study of textured (110)-oriented LSM films on (111) YSZ,[36] we found strong correlation between two parallel paths that could be assigned to the native surface and the grain boundaries. Similar to here, the behavior was complex with temperature depending on their overall contributions. What thin films offer in this regard is the possibility of controlling for different structural features in a straightforward manner, ultimately allowing their effects on surface chemistry to be unravelled.

Here we reported values only for (100) films. In a prior report,[37] we showed that for relaxed films on STO (600 nm) having (100), (111), and (110) surface orientations, both the overall k_{chem} and the activation energies were orientation dependent. While the nature of the (100) surface at 600 nm appears to be mediated by dislocations based on the current work, we infer the same is true for relaxed films on STO with other orientations. Since the nature of the dislocation-free surfaces for other orientations is still unknown, we cannot be sure of the relative contribution the dislocations make on specific orientation without further work.

The relationship of thin film work to real fuel cells is also of interest. Here we can isolate the effects of different microstructural and chemical parameters on overall surface exchange (or the oxygen reduction reaction at open circuit). These results imply the local activity should vary greatly depending on the local strain states, surface states, and proximity to an extended defect (not only triple phase boundary lines but also grain boundaries and dislocations), as well as each of these varying with temperature. This indicates the surface activity is widely varying, which has potential for both the average activity but also the local degradation. Also, much recent work in SOFCs has focused on decorating micrometer-sized pore surfaces with nanoscale catalysts, which are similar in size to the films under investigation. A recent study showed that a $(La,Sr)MnO_3$ thin film coating[91] on $(La,Sr)(Co,Fe)O_3$ cathodes led to surfaces possessing better structural and chemical stability for SOFC operation. In other words, thin film samples not only offer an ability to control parameters that directly impact surface chemical processes in a meaningful fashion, but they are more and more relevant to complex catalysts under design for use in SOFCs. Our work indicates that, at least for (100) surfaces, activity can be improved at high temperatures through tensile strain, while at intermediate temperatures by increasing the extended defect populations.

5. CONCLUSIONS

In summary, epitaxial $La_{0.7}Sr_{0.3}MnO_3$ films with well-controlled surface properties were prepared on $SrTiO_3$ and $NdGaO_3$ substrates. Several interesting observations were found. First, two distinct activation energies (E_a) were found for k_{chem}, indicating two parallel mechanisms contribute to surface exchange in LSM films. E_a for surface regions that are influenced by the presence of extended defects intersecting the surface was ~0.75 eV, found for thick relaxed films. For surface regions free of dislocations, $E_a \approx 1.5$ eV, which was found for thin coherently strained films. Second, significant substrate effects were observed to impact k_{chem}, which varied by over 3 orders of magnitude depending on substrate, thickness, and temperature. In 50 nm films, k_{chem} of films on STO is 1 order of magnitude larger than on NGO at all temperatures. In 600 nm thick films, k_{chem} of films on $SrTiO_3$ is larger than on $NdGaO_3$ by a factor of 2, at all temperatures. Third, the relative contributions from the two mechanisms depend on substrate, thickness and temperature. For thin films, homogeneous strain strongly impacts the relaxation time; and it reveals the intrinsic surface responses. For thick films, extended defect determines the relaxation time; and it is related to dislocation density and activity. The relative contribution of the dislocation mediated mechanism maximized in intermediate temperature ranges. We proposed a model that is consistent with the structural properties and surface exchange data.

■ ASSOCIATED CONTENT

Supporting Information

Figure S1 gives a representative fit to transient conductivity data for the 100 nm film on $SrTiO_3$ at 600 °C. Figure S2 gives the steady state conductivity as a function of temperature for 50 and 600 nm films on STO (100) and NGO (110); the inset shows the steady-state conductivity as a function of oxygen partial pressure of 600 nm LSM film on STO (100).[37] Figure S3 gives the surface exchange coefficients of 50 and 600 nm films on STO (100) and NGO (110) as a function of film thickness during both oxidation and reduction processes. This material is available free of charge via the Internet at http://pubs.acs.org.

■ AUTHOR INFORMATION

Corresponding Author

*E-mail: paulsalvador@cmu.edu.

Author Contributions

The manuscript was written through contributions of all authors. All authors have given approval to the final version of the manuscript.

Notes

The authors declare no competing financial interest.

■ ACKNOWLEDGMENTS

This work was supported by the U.S. Department of Energy under Award DE−NT0004117 through the Strategic Energy Conversion Alliance (SECA) program.

■ REFERENCES

(1) Minh, N. Q.; Takahashi, T. *Science and Technology of Ceramic Fuel Cells*; Elsevier Science: Amsterdam, 1995.
(2) Adler, S. B. *Chem. Rev.* **2004**, *104*, 4791.
(3) Jacobson, A. J. *Chem. Mater.* **2009**, *22*, 660.
(4) Maier, J. *Physical Chemistry of Ionic Materials*; John Wiley & Sons: New York, 2004.
(5) la O', G. J.; Ahn, S. J.; Crumlin, E.; Orikasa, Y.; Biegalski, M. D.; Christen, H. M.; Shao-Horn, Y. *Angew. Chem., Int. Ed.* **2010**, *49*, 5344.
(6) Vohs, J. M.; Gorte, R. J. *Adv. Mater.* **2009**, *21*, 943.
(7) Fleig, J. *Ann. Rev. Mater. Res.* **2003**, *33*, 3361.
(8) Fleig, J.; Maier, J. *J. Eur. Ceram. Soc.* **2004**, *24*, 1343.
(9) Fleig, J.; Baumann, F. S.; Brichzin, V.; Kim, H. R.; Jamnik, J.; Cristiani, G.; Habermeier, H. U.; Maier, J. *Fuel Cells* **2006**, *6*, 284.
(10) Kim, G.; Wang, S.; Jacobson, A. J.; Chen, C. L. *Solid State Ionics* **2006**, *177*, 1461.
(11) Kim, G.; Wang, S.; Jacobson, A. J.; Yuan, Z.; Donner, W.; Chen, C. L.; Reimus, L.; Brodersen, P.; Mims, C. A. *Appl. Phys. Lett.* **2006**, *88*, 024103.
(12) Yan, L.; Kavaipatti, B. P.; Wang, S.; Du, H.; Salvador, P. *Mater. Res. Soc. Symp. Proc.* **2010**, 1255.
(13) Garcia, G.; Burriel, M.; Bonanos, N.; Santiso, J. *J. Electrochem. Soc.* **2008**, *155*, P28.
(14) Burriel, M.; Garcia, G.; Santiso, J.; Kilner, J. A.; Richard, J. C. C.; Skinner, S. J. *J. Mater. Chem.* **2008**, *18*, 416.
(15) la O', G. J.; Shao-Horn, Y. *J. Electrochem. Soc.* **2009**, *156*, B816.
(16) Fleig, J.; Kim, H. R.; Jamnik, J.; Maier, J. *Fuel Cells* **2008**, *8*, 330.
(17) la O', G. J.; Shao-Horn, Y. *Electrochem. Solid State Lett.* **2009**, *12*, B82.
(18) Wang, W.; Jiang, S. P. *Solid State Ionics* **2006**, *177*, 1361.
(19) Wang, W.; Jiang, S. P. *J. Solid State Electrochem.* **2004**, *8*, 914.
(20) Jiang, S. P.; Love, J. G. *Solid State Ionics* **2001**, *138*, 183.
(21) Jiang, S. P.; Love, J. G. *Solid State Ionics* **2003**, *158*, 45.
(22) Jiang, S. P.; Wang, W. *Electrochem. Solid State Lett.* **2005**, *8*, A115.
(23) Bertacco, R.; Contour, J. P.; BarthÈlemy, A.; Olivier, J. *Surf. Sci.* **2002**, *511*, 366.
(24) Fister, T. T.; Fong, D. D.; Eastman, J. A.; Baldo, P. M.; Highland, M. J.; Fuoss, P. H.; Balasubramaniam, K. R.; Meador, J. C.; Salvador, P. A. *Appl. Phys. Lett.* **2008**, 93.
(25) Katsiev, K.; Yildiz, B.; Balasubramaniam, K.; Salvador, P. A. *Appl. Phys. Lett.* **2009**, *95*, 092106.
(26) Chang, K.-C. I., B.; Balasubramaniam, K. R.; Yildiz, B.; Hennessy, D.; Salvador, P. A.; Leyarovska, N.; You, H. *Mater. Res. Soc. Symp. Proc.* **2009**, 1126.
(27) Jeong Woo, H.; Helia, J.; Yener, K.; Zhuhua, C.; Bilge, Y. *ECS Trans.* **2010**, *35*, 2097.
(28) Jalili, H.; Han, J. W.; Kuru, Y.; Cai, Z.; Yildiz, B. *J. Phys. Chem. Lett.* **2011**, *2*, 801.
(29) Baumann, F. S.; Fleig, J.; Konuma, M.; Starke, U.; Habermeier, H.-U.; Maier, J. *J. Electrochem. Soc.* **2005**, *152*, A2074.
(30) Lee, Y.-L.; Kleis, J.; Rossmeisl, J.; Morgan, D. *Phys. Rev. B* **2009**, *80*, 224101.
(31) Kushima, A.; Yip, S.; Yildiz, B. *Phys. Rev. B* **2010**, 82.
(32) Klenov, D. O.; Donner, W.; Foran, B.; Stemmer, S. *Appl. Phys. Lett.* **2003**, *82*, 3427.
(33) Donner, W.; Chen, C.; Liu, M.; Jacobson, A. J.; Lee, Y.-L.; Gadre, M.; Morgan, D. *Chem. Mater.* **2011**, *23*, 984.
(34) Karthikeyan, A.; Ramanathan, S. *Appl. Phys. Lett.* **2008**, *92*, 243109.
(35) Chen, L.; Chen, C. L.; Jacobson, A. J. *IEEE Trans. Appl. Supercon.* **2003**, *13*, 2882.
(36) Yan, L.; Kavaipattib, B.; Chang, K.-C.; You, H.; Salvador, P. *ECS Trans.* **2011**, *35*, 2063.
(37) Yan, L.; Balasubramaniam, K. R.; Wang, S.; Du, H.; Salvador, P. A. *Solid State Ionics* **2011**, *194*, 9.
(38) Chen, X.; Wang, S.; Yang, Y. L.; Smith, L.; Wu, N. J.; Kim, B.-I.; Jacobson, S. S. P. A. J.; Ignatiev, A. *Solid Sates Ionics* **2002**, *146*, 405.
(39) Tal, Z. S.; Chun, L.; Craig, P. J.; Steven, J. V.; Lutgard, C. D. J. *Electrochem. Solid State Lett.* **2006**, *9*, A376.
(40) Zhang, Q. S.; Hirano, A.; Matsumura, T.; Imanishi, N.; Takeda, Y.; Yamahara, K. *J. Fuel Cell Sci. Technol.* **2009**, *6*, 011010.
(41) Du, H. Processing, Microstructure, and Tunable Microwave Dielectric Properties of (Ba,Sr)TiO_3 Thin Films. Carnegie Mellon University, Pittsburgh, PA, 2009.
(42) Balasubramanian, K. R.; Chang, K.-C.; Mohammad, F. A.; Porter, L. M.; Salvador, P. A.; DiMaio, J.; Davis, R. F. *Thin Solid Films* **2006**, *515*, 1807.
(43) Andrew, J. F.; Paul, A. S. *J. Appl. Phys.* **2004**, *96*, 2482.
(44) Du, H.; Fisher, P. J.; Skowronski, M.; Salvador, P. A.; Maksimov, O. *J. Cryst. Growth* **2008**, *310*, 1991.
(45) Sasaki, K.; Maier, J. *Solid State Ionics* **2003**, *161*, 145.
(46) Arturas, V.; Hans, B.; Evert, H.; Gertjan, K.; Guus, R.; Dave, H. A. B. *Appl. Phys. Lett.* **2009**, *95*, 152508.
(47) Wollan, E. O.; Koehler, W. C. *Phys. Rev.* **1955**, *100*, 545.
(48) Ovsyannikov, G.; Petrzhik, A.; Borisenko, I.; Klimov, A.; Ignatov, Y.; Demidov, V.; Nikitov, S. *J. Exp. Theor. Phys.* **2009**, *108*, 48.
(49) Martin, M. C.; Shirane, G.; Endoh, Y.; Hirota, K.; Moritomo, Y.; Tokura, Y. *Phys. Rev. B* **1996**, *53*, 14285.
(50) Maurice, J. L.; Pailloux, F.; Barthelemy, A.; Durand, O.; Imhoff, D.; Lyonnet, R.; Rocher, A.; Contour, J. P. *Phil. Mag.* **2003**, *83*, 3201.
(51) Urushibara, A.; Moritomo, Y.; Arima, T.; Asamitsu, A.; Kido, G.; Tokura, Y. *Phys. Rev. B* **1995**, *51*, 14103.
(52) Jonker, G. H. *Physica* **1956**, *22*, 707.
(53) Farrel, W. L. *J. Appl. Phys.* **1964**, *35*, 2212.
(54) Loetzsch, R.; Lubcke, A.; Uschmann, I.; Forster, E.; Grosse, V.; Thuerk, M.; Koettig, T.; Schmidl, F.; Seidel, P. *Appl. Phys. Lett.* *96*, 071901.
(55) Goodenough, J. B.; Longo, J. M., Crystallographic and Magnetic Properties of Perovskite and Perovskite-Related Compounds. In *Magnetic and Other Properties of Oxides and Related Compounds*; Hellwege, K.-H., Madelung, O., Eds.; Springer: Berlin, 1970.
(56) Geller, S. *Acta Crystallogr.* **1957**, *10*, 243.

(57) Marti, W.; Fischer, P.; Schefer, J.; Kubel, F. *Z. Kristallogr.* **1996**, *211*, 891.
(58) Kleptsyn, V.; Guenrikhson, V.; Bogunov, V. *J. Cryst. Growth* **1997**, *171*, 109.
(59) Vasylechko, L.; Akselrud, L.; Morgenroth, W.; Bismayer, U.; Matkovskii, A.; Savytskii, D. *J. Alloys Compd.* **2000**, *297*, 46.
(60) People, R.; Bean, J. C. *Appl. Phys. Lett.* **1985**, *47*, 322.
(61) Solis, C.; Jung, W.; Tuller, H. L.; Santiso, J. *Chem. Mater.* **2010**, *22*, 1452.
(62) Nishikawa, H.; Houwman, E.; Boschker, H.; Mathews, M.; Blank, D. H. A.; Rijnders, G. *Appl. Phys. Lett.* **2009**, *94*, 042502.
(63) Halliwell, M. A. G. *Appl. Phys. A: Mater. Sci. Process.* **1994**, *58*, 135.
(64) Ayers, J. E. *J. Cryst. Growth* **1994**, *135*, 71.
(65) Yarlagadda, B.; Rodriguez, A.; Li, P.; Velampati, R.; Ocampo, J. F.; Suarez, E. N.; Rago, P. B.; Shah, D.; Ayers, J. E.; Jain, F. C. *Appl. Phys. Lett.* **2008**, *92*, 202103.
(66) Ehrlich, G.; Stolt, K. *Annu. Rev. Phys. Chem.* **1980**, *31*, 603.
(67) Hoefnagels, J. P. M.; Langereis, E.; Kessels, W. M. M.; van de Sanden, M. C. M. *IEEE Trans. Plasma Sci.* **2005**, *33*, 234.
(68) Mizusaki, J.; Yonemura, Y.; Kamata, H.; Ohyama, K.; Mori, N.; Takai, H.; Tagawa, H.; Dokiya, M.; Naraya, K.; Sasamoto, T.; Inaba, H.; Hashimoto, T. *Solid State Ionics* **2000**, *132*, 167.
(69) Kuo, J. H.; Anderson, H. U.; Sparlin, D. M. *J. Solid State Chem.* **1990**, *87*, 55.
(70) Poulsen, F. W. *Solid State Ionics* **2000**, *129*, 145.
(71) Yan, L.; Kavaipatti, B. P.; Wang, S.; Du, H.; Salvador, P., Effects of Film Thickness and Substrate Related Strain States on Catalytic Activity of SOFC Cathode Materials. In *Proceedings of the 218th Electrochemical Society Meeting*; Las Vegas, NV, Oct 10−15, 2010 ; Electrochemical Society: Pennington, NJ, 2010.
(72) Tsuchiya, M.; Bojarczuk, N. A.; Guha, S.; Ramanathan, S. *J. Chem. Phys.* **2009**, 130.
(73) Kan, C. C.; Wachsman, E. D. *Solid State Ionics* **2010**, *181*, 338.
(74) Belzner, A.; Gür, T. M.; Huggins, R. A. *Solid State Ionics* **1992**, *57*, 327.
(75) Chopdekar, R. V.; Arenholz, E.; Suzuki, Y. *Phys. Rev. B* **2009**, *79*, 104417.
(76) Tebano, A.; Orsini, A.; Castro, D. D.; Medaglia, P. G.; Balestrino, G. *Appl. Phys. Lett.* **2010**, *96*, 092505.
(77) Sun, J. R.; Yeung, H. W.; Wong, H. K.; Zhu, T.; Shen, B. G. *Eur. Phys. J. B* **2003**, *35*, 481.
(78) Mizusaki, J.; Mima, Y.; Yamauchi, S.; Fueki, K.; Tagawa, H. *J. Solid State Chem.* **1989**, *80*, 102.
(79) Cratty, L. E.; Granato, A. V. *J. Chem. Phys.* **1957**, *26*, 96.
(80) Uhara, I.; Adachi, G.; Tani, K.; Yanagimo, S. *Nature* **1961**, *192*, 867.
(81) Hall, J. W.; Rase, H. F. *Nature* **1963**, *199*, 585.
(82) Uhara, I.; Kishimoto, S.; Yoshida, Y.; Hikino, T. *J. Phys. Chem.* **1965**, *69*, 880.
(83) de la Figuera, J.; Pohl, K.; Schmid, A. K.; Bartelt, N. C.; Hwang, R. Q. *Surf. Sci.* **1998**, *415*, L993.
(84) Wintterlin, J.; Zambelli, T.; Trost, J.; Greeley, J.; Mavrikakis, M. *Angew. Chem., Int. Ed.* **2003**, *42*, 2850.
(85) Szot, K.; Speier, W.; Bihlmayer, G.; Waser, R. *Nat. Mater.* **2006**, *5*, 312.
(86) Otsuka, K.; Kuwabara, A.; Nakamura, A.; Yamamoto, T.; Matsunaga, K.; Ikuhara, Y. *Appl. Phys. Lett.* **2003**, *82*, 877.
(87) Klie, R. F.; Walkosz, W.; Yang, G.; Zhao, Y. *J. Electron Microsc.* **2009**, *58*, 185.
(88) Jiang, W.; Evans, D.; Bain, J. A.; Skowronski, M.; Salvador, P. A. *Appl. Phys. Lett.* **2010**, 96.
(89) la O', G. J.; Yildiz, B.; McEuen, S.; Shao-Horn, Y. *J. Electrochem. Soc.* **2007**, *154*, B427.
(90) Fuchigami, K.; Gai, Z.; Ward, T. Z.; Yin, L. F.; Snijders, P. C.; Plummer, E. W.; Shen, J. *Phys. Rev. Lett.* **2009**, *102*, 066104.
(91) Choi, J.-J.; Qin, W.; Liu, M.; Liu, M. *J. Am. Ceram. Soc.* **2011**, *94*, 3340.